THERMAL DIFFUSIVITY AND SOUND VELOCITY OF THE REFRIGERANT R143A (1,1,1-TRIFLUOROETHANE)[1]

A. P. Fröba[2], S. Will[3], and A. Leipertz [2,4]

---

[1] Paper presented at the Fourteenth Symposium on Thermophysical Properties, June 25-30, 2000, Boulder, Colorado, U.S.A.

[2] Lehrstuhl für Technische Thermodynamik (LTT), Friedrich-Alexander-Universität Erlangen-Nürnberg, Am Weichselgarten 8, D-91058 Erlangen, Germany

[3] Technische Thermodynamik / Wärme- und Stofftransport (TTWSt), Universität Bremen, FB4, Badgasteiner Straße 1, D-28359 Bremen, Germany

[4] Author to whom correspondence should be addressed.

ABSTRACT

The thermal diffusivity and the sound velocity of the refrigerant R143a (1,1,1-Trifluoroethane) have been determined in the temperature range 273-346 K by dynamic light scattering (DLS), a method based on the time-resolved analysis of scattered light intensities, which are caused by microscopic density fluctuations in the sample. The results for R143a are discussed in detail in comparison to data being available in the literature. With the help of reference data for the thermal conductivity and density our experimental data of the thermal diffusivity also allow the derivation of the isobaric heat capacity for both phases under saturation conditions.

KEY WORDS: dynamic light scattering; R143a; sound velocity; thermal diffusivity.

1. INTRODUCTION

In connection with the prohibition of chlorinated hydrocarbons (CFCs) based on the Montreal protocol the chlorine-free HFCs R23 (Trifluoromethane), R125 (Pentafluoroethane), R32 (Difluoromethane), R134a (1,1,1,2-Tetrafluoroethane), R152a (1,1-Difluoroethane) and R143a (1,1,1-Trifluoroethane) evolved as long-term alternatives. On account of their thermodynamic properties and of safety requirements all the aforementioned substances, except for R134a that is used as a direct substitute of R12 in domestic appliances, are employed as mixtures in almost all fields of refrigeration and air conditioning.

In the last years intensive international activities have been carried out in order to rapidly provide comprehensive data sets for the thermophysical properties of all possibly relevant substitutes for the fully-chlorinated hydrocarbons used previously. As it is not possible for these mixtures to experimentally determine a great number of properties in a large variety of thermodynamic states, models are employed for the design of apparatus in refrigeration and air conditioning systems, which are based on the data of the pure substances.

After ten years of research most of the data for the class of partially fluorated hydrocarbons are available for R134a and for R152a. In contrast, a literature survey reveals that only a very limited number of data are available for refrigerant R143a, which for refrigeration purposes is mainly used as a component in the blends R404A (R125/R134a/R143a) and R507 (R125/R143a). This situation holds both for equilibrium data and even more pronounced for transport properties. Thus, only two experimental data sets can be found in the literature for the thermal conductivity of both saturated liquid and vapor [1-3], and data for the upper temperature region are only obtained

from lower temperature values by extrapolation and are completely lacking for the critical region.

In the present paper the methodological principles of dynamic light scattering (DLS) for the determination of thermal diffusivity and sound velocity are briefly reviewed. Then experimental results for R143a are discussed in comparison with the few literature data available.

2. METHOD

In the following the underlying theory of DLS from bulk fluids is briefly introduced. For a more detailed and comprehensive description the reader is referred to the literature [4-7].

When a fluid sample in macroscopic equilibrium is irradiated by coherent laser light, light scattered from the sample can be observed in all directions. The underlying scattering process is governed by microscopic fluctuations of the thermodynamic properties temperature and pressure, and of species concentration in binary mixtures. The relaxations of these statistical fluctuations follow the same laws which are valid for macroscopic systems. Thus, the decay of temperature fluctuations is governed by the thermal diffusivity a. Pressure fluctuations in fluids are moving with sound velocity c_S and are damped by the sound attenuation D_S, and in fluid mixtures fluctuations in concentration are decaying in dependence on the mutual diffusion coefficient D_{12}.

A typical scattering geometry for light scattering from bulk fluids is shown in Fig. 1. With the scattering angle Q_s, which defines the angle between the direction of observation and incident light, the scattering vector is determined by $\vec{q} = \vec{k}_i - \vec{k}_s$. Here, the

wave vectors of incident and scattered light are represented by $\vec{k}_i$ and $\vec{k}_s$, respectively. Assuming elastic scattering ($k_i \cong k_s$), the modulus of the scattering vector is given by the fluid refractive index *n*, the laser wavelength in vacuo l_0 and the scattering angle Q_s by

$$q = \left|\vec{k}_i - \vec{k}_s\right| \cong 2\, k_i \sin(Q_s/2) = \frac{4pn}{l_0} \sin(Q_s/2)\,. \qquad (1)$$

In light scattering experiments the above-mentioned equalization processes result in a temporal modulation of the scattered light intensity. Information about these processes can be derived by a temporal analysis of the scattered light using photon correlation spectroscopy. For heterodyne conditions, where a reference beam is superimposed on the scattered light, the correlation function for the analysis of the temperature fluctuations is described by

$$G^{(2)}(t) = A + B\exp(-t/t_C)\,. \qquad (2)$$

From the correlation time t_C, which is equivalent to the mean life time of the temperature fluctuations observed, the thermal diffusivity *a* can be calculated by

$$a = \frac{1}{t_C q^2}\,. \qquad (3)$$

For the measurement of sound velocity c_S the pressure fluctuations are probed. In practice, the frequency w_S of the sound waves is determined by adding a reference beam,

which is shifted relative to w_S by Δw_M applying an acousto-optical modulator. The frequency shift Δw_M is of the same order of magnitude as the frequency of the sound waves ($\Delta w_M \approx w_S$). In this case, the correlation function takes the form

$$G^{(2)}(t) = A + B\exp(-t / t_C)\cos(\Delta w t), \tag{4}$$

where the sound velocity c_S can be found from the adjusted modulator frequency Δw_M and the residual detuning Δw according to

$$c_S = \frac{w_S}{q} = \frac{\Delta w_M \pm \Delta w}{q}. \tag{5}$$

Furthermore, the sound attenuation D_S can be determined from the decay time t_C of the correlation function Eq. (4) by

$$D_S = \frac{1}{t_C q^2}. \tag{6}$$

3. EXPERIMENTAL

The experimental set-up used is shown schematically in Fig. 2. Light from an argon-ion laser operating at a single longitudinal mode at a wavelength of l_0 = 488 nm irradiates a liquid sample inside a pressure vessel through a quartz window. The laser power was up to 300 mW when working far away from the critical point, and only a few mW in the critical region. The observation direction is given by two stops at a distance of about 4 m. The scattered light is

typically detected at small angles Q_s ~ 3-5°. For large scattering intensities from the sample the scattered reference light from the cell windows is not sufficient to realize heterodyne conditions. Here, an additional reference beam is added. To this end, part of the incident laser light is splitted by a glass plate and superimposed to the scattered light behind the sample cell. Additionally, for the determination of sound velocity, the reference beam can be shifted in frequency by a single opto-acoustic modulator or by a combination of modulators to reach the desired frequency shift Δw_M. The scattered light intensities are detected by two photomultiplier tubes (PMT's), and the cross-correlation function employed in order to suppress afterpulsing effects, is calculated by a digital correlator. A stand-alone correlator with 112 linearily spaced channels was used operated with a sample time of down to 100 ns for the determination of sound velocity. For the measurement of thermal diffusivity, the sample time was chosen in a way that the correlation function covers about six decay times.

With the help of Snell's refraction law and simple trigonometric identities it can be shown that from the angle of incidence Q_i, which is defined as the angle between the optical axes of incidence laser beam and detection direction (see Fig. 2), the scattering vector q can be deduced to be

$$q \cong \frac{2p}{l_0} \sin Q_i \qquad (7)$$

and can thus be calculated without knowledge of the refractive index n of the sample. The error in the desired quantities resulting from the approximation Eq. (7) is below 0.1 % for angles of incidence up to 5 degrees. In the present experiments the angle of

incidence has been measured with an accuracy of approximately ± 0.014 degree by back-reflection from a mirror, mounted on a precision rotation table.

According to an analysis of the manufacturer (Solvay Fluor und Derivate GmbH, Hannover) the refrigerant sample had a purity of 99.99 % and was used without further purification. The sample was filled from the vapor phase into an evacuated cylindrical pressure vessel (volume, ≈ 10 cm^3) equipped with two quartz windows (Herasil I; diameter, 30 x 30 mm). The actual temperature in the sample cell, which was placed in a multi-stage-thermostat surrounded by an insulating housing, was regulated through resistance heating and showed a long-term stability of better than ± 0.002 K. The temperature of the sample was measured with three calibrated 25-*W* platinum resistance probes, integrated in the main body of the measuring cell, with an uncertainty of ± 0.015 K. For temperatures below room temperature, the insulating housing was cooled about 10 K below the desired temperature in the sample cell. For each temperature point, typically six measurements at different angles of incidence were performed, where the laser was irradiated from either side with respect to the axis of observation in order to check for a possible misalignment.

4. RESULTS AND DISCUSSION

4.1 Thermal Diffusivity

The results of the measurements of the thermal diffusivity for the saturated liquid and saturated vapor phase are summarized in Table I and Fig. 3. Each temperature point comprises six single measurements, the mean value of which is displayed. The continuous lines are empirical correlations of the experimental data. Either data set can - within experimental uncertainty - be represented by the sum of a polynomial and an additionally necessary term which explicitly accounts for the critical behavior,

$$a = \sum_{i=0}^{3} a_i \left(\frac{T}{K} \right)^i + a_4 \left(\frac{T_c - T}{T_c} \right)^{0.67}, \qquad (8)$$

where the critical temperature of T_c = 346.25 K was taken from Ref. 9. This value is in agreement with the observed maximum opalescence of the sample at a temperature of 346.22 ± 0.03 K. Table II summarizes the coefficients of Eq. (8) for either phase under saturation conditions. Here, also the root-mean square deviations of our values from Eq. (8) and the ranges of validity of the correlations are stated.

In the residual plot of Fig. 3 for the liquid phase error bars are exemplarily depicted, which represent the standard deviation of the single measurements and which may be regarded as measure for the uncertainty of DLS data [10]. For the saturated liquid, a standard deviation of about 2 % was obtained for temperatures below 300 K and of mostly below 1% for temperatures above. The observed behavior can be explained with an increasing signal

amplitude for higher temperatures. A corresponding observation regarding the standard deviation holds for the saturated vapor phase. In approaching the critical point the standard deviation increases to a value of again about 2 %, which is due to increasing experimental complexities in the critical region. Thus, investigations in the close vicinity of the gas-liquid critical point require additional effort, which was not done here. Furthermore, due to long measurement times at lower temperatures, the data for the thermal diffusivity in the vapor phase had to be restricted to temperatures above 318 K.

In Fig. 3, for the saturated liquid, reference data from thermal conductivity measurements have been included, which have been converted to thermal diffusity according to

$$a = \frac{l}{r\, c_{\mathrm{p}}}, \tag{9}$$

using values for the isobaric heat capacity c_{p} of Günther and Steimle [11] and for the density r of Widiatmo et al. [12]. A direct comparison is not possible for either phase due to a lack of corresponding reference data for the thermal diffusivity. For the boiling liquid, the thermal conductivity data of Yata et al. [1] and Hoffmann et al. [2], both of them obtained by the transient hot wire method, deviate from our correlation in a range of about -4 % to +3 %. These differences are within the combined uncertainties of the methods, if one takes the uncertainty of the heat capacity data of below 1 % for temperatures up to 313 K and below 2 % for the temperature range between 313 K to 323 K, according to Ref. 11, into account. The basically similar course of the deviations for either data set is founded in the correlation of

the thermal conductivity data through a linear regression in temperature by the respective authors.

For the thermal diffusivity of the vapor phase under saturation a data comparison has not been possible due to a lack of values for the isobaric heat capacity. On the other hand, however, a derivation of this quantity under saturation is possible with the present thermal diffusivity data and with the help of reference data for the thermal conductivity and the density in the vapor phase, see, e.g. Refs. 3 and 13, respectively. The result of this procedure is shown in Fig. 4.

4.2 Sound Velocity

Our results from dynamic light scattering for the sound velocity of saturated R143a are summarized in Table III and Fig. 5. The sound velocity data for both vapor and liquid phase can well be represented by a sum of a linear and an additional term, which takes into account the curvature towards the critical point, resulting in an equation of the form

$$c_S = c_0 + c_1\left(\frac{T}{K}\right) + c_2\left(\frac{T_c - T}{T_c}\right)^{\varphi} \qquad (10)$$

where the coefficients c_i and the additional fit parameter φ are given in Table IV. The critical temperature again was adopted from Ref. 9. For both phases the root-mean square deviation of our data from the fit according to Eq. (10) is clearly below 0.5% over the whole temperature range.

Taking into account the major error sources, the uncertainty of the sound velocity data for temperatures not to close too the critical point ($T/T_c < 0.99$) can be estimated to be below ± 0.5%. For the highest temperatures studied in this work the overall uncertainty for the sound velocity increases to a value of about 1% as represented by the error bars in Fig. 5. The reason for this behavior can again be found by an increasing experimental complexity in the critical region. It should also be noted that the measured sound velocities are naturally not in the thermodynamic $w_S = 0$ limit, and thus, dispersion might affect both average values and standard deviation.

For comparison of the sound velocity of the liquid phase under saturation conditions only one data set is available in literature. These are estimated values by Takagi [14], where the sound velocity on the saturation line is obtained by extrapolating experimental data for the compressed liquid phase measured with an ultrasonic acoustic interferometer. In Ref. 14 an estimated uncertainty of ± 0.2% for the experimental values in the high density region is stated, yet due to absorption effects at higher temperatures near the saturation region a larger error, especially for the sound velocity below 400 $m \cdot s^{-1}$, is mentioned. These facts may explain that at a temperature of about 300 K, where the sound velocity is 400 $m \cdot s^{-1}$, an increasing difference between our data and the estimation given by Takagi can be observed with increasing temperature, see Fig 5. As far away from the critical point Eq. (10) well reflects the quasi-linear temperature dependence of the saturated liquid sound velocity, we have extrapolated our correlation for temperatures down to 250 K. Here, better agreement can be found between the extrapolated data and those given by Takaki [14].

Though experimental data exist in the literature for gas-phase sound velocities of R143a, see, e.g. Ref. 15 and 16, no data are available for the saturation line. Thus, no data comparison was performed here.

5. CONCLUSIONS

For the refrigerant R143a, which serves as one principal component in the refrigerant blends R507 and R404A, thermal diffusivity and sound velocity have been measured using dynamic light scattering. Values have been determined for both the liquid and vapor phase under saturation conditions over a wide temperature range up to the critical point. For a limited range at moderate temperatures, where reference data in the liquid phase are available for density, thermal conductivity, and the specific heat, a comparison with our thermal diffusivity data shows agreement within the cumulative errors of the single properties used for data conversion. In the high temperature range a comparison of our results obtained for the thermal diffusivity and sound velocity was not possible due to the lack of other data sets in this region. Here, experiments by other techniques would be most helpful. For the thermal diffusivity and sound velocity of R143a, to the best of our knowledge, the present results from dynamic light scattering are the first experimental values under saturation conditions.

ACKNOWLEDGEMENTS

Part of the work was financially supported by the Deutsche Forschungsgemeinschaft (DFG). The authors gratefully acknowledge the help of Solvay Fluor und Derivate GmbH, Hannover, by providing the refrigerant sample and analyzing the purity.

REFERENCES

[1] J. Yata, M. Hori, K. Kobayashi, and T. Minamiyama, *Int. J. Thermophys.* **17**:561 (1996).

[2] N. Hoffmann, K. Spindler, and E. Hahne, *Bestimmung der Transportgrößen von HFKW*, Bericht zum AiF-Forschungsvorhaben Nr. 10044B, Forschungsrat Kältetechnik e.V., ed. (Frankfurt, 1996), pp. 23-24.

[3] Y. Tanaka, M. Nakata, and T. Makita, *Int. J. Thermophys.* **12**:949 (1991).

[4] A. Leipertz, *Fluid Phase Equil.* **125**:219 (1996).

[5] S. Will and A. Leipertz, in *Diffusion in Condensed Matter*, J. Kärger, P. Heitjans, and R. Haberlandt, eds. (Vieweg, Wiesbaden, 1999), pp. 219-244.

[6] B. J. Berne and R. Pecora, *Dynamic Light Scattering*, John Wiley, New York (1976).

[7] B. Chu , *Laser Light Scattering*, Academic Press, New York (1991).

[8] K. Kraft and A. Leipertz, *Int. J. Thermophys.* **16**:445 (1995).

[9] M. O. McLinden, *Int. J. Refrig.* **13**:149 (1990).

[10] K. Kraft, M. Matos Lopes, and A. Leipertz, *Int. J. Thermophys.* **16**:423 (1995).

[11] D. Günther and D. Steimle, *DKV-Tagungsbericht 23* (Leipzig, 1996), Vol. II.1 pp. 261-272.

[12] J. V. Widiatmo, H. Sato, and K. Watanabe, *J. Chem. Eng. Data* **39**:304 (1994).

[13] K. Srinivasan and L. R. Oellrich, *Int. J. Refrig.* **20**:332 (1997).

[14] T. Takagi, *J. Chem. Eng. Data* **42**:1129 (1997).

[15] K. A. Gillis, *Int. J. Thermophys.* **18**:73 (1997).

[16] T. Ichikawa, T. Hozumi, K. Ogawa, H. Sato, and K. Watanabe, “Speed of sound measurements for Gaseous 1,1,1-Trifluoroethane (R143a)”, to be submitted to *Int. J. Thermophys.*, 1999.

Table I: Experimental Values of the Thermal Diffusivity *a* of R143a (1,1,1-Trifluoro-ehtane) Under Saturation Conditions.

Liquid phase		Vapor phase	
T , K	*a*, 10^{-8} $m^2 \cdot s^{-1}$	*T*, K	*a*, 10^{-8} $m^2 \cdot s^{-1}$
273.05	5.25	318.12	10.32
283.30	4.79	320.57	9.38
293.03	4.52	323.10	8.60
298.10	4.32	325.60	7.70
303.15	4.19	328.10	6.83
308.13	4.00	330.59	5.87
313.10	3.86	333.10	5.00
318.07	3.65	335.59	4.13
323.03	3.43	338.09	3.24
328.01	3.15	341.09	2.16
330.09	2.96	343.08	1.33
333.09	2.71	344.08	0.941
336.09	2.39	345.08	0.527
338.09	2.15		
340.08	1.83		
341.08	1.64		
342.08	1.42		
343.08	1.16		
344.08	0.846		
345.08	0.462		

Table II: Coefficients of Eq. (8).

a_i, 10^{-8} $m^2 \cdot s^{-1}$	Liquid phase	Vapor phase
a_0	49.5183	142.7971
a_1	-0.733715	-0.558964
a_2	2.288873×10^{-3}	0.422476×10^{-3}
a_3	-1.695681×10^{-6}	—
a_4	56.455	13.812
rms, %	0.53	0.77
T-range, K	273-345	318-345

Table III: Experimental Values of the Sound Velocity c_S of R143a (1,1,1-Trifluoro-ehtane) Under Saturation Conditions.

Liquid phase		Vapor phase	
T , K	c_S, m·s^{-1}	T, K	c_S, m·s^{-1}
288.11	449.5	313.13	136.8
293.11	425.2	318.12	132.4
297.95	401.0	323.11	128.5
303.14	373.0	328.10	123.4
308.10	347.0	333.10	118.5
313.06	319.7	336.10	115.0
318.03	291.0	339.10	111.0
322.98	262.3	341.10	107.9
328.80	228.8	343.10	104.4
333.09	199.4	344.10	101.9
338.09	163.5	345.10	98.45
340.23	145.7	345.60	95.79
342.84	123.1		
342.90	121.7		
344.04	110.8		
344.99	99.77		

Table IV: Coefficients of Eq. (10).

c_i, $m \cdot s^{-1}$	Liquid phase	Vapor phase
c_0	978.29	281.696
c_1	-2.6095	-0.60365
c_2	665.96	65.547
φ	0.612	0.1685
rms, %	0.29	0.10
T-range, K	288-345	313-345

FIGURE CAPTIONS

Fig. 1 Scattering geometry: light scattering from bulk fluids.

Fig. 2 Experimental setup.

Fig. 3 Thermal diffusivity of saturated R143a.

Fig. 4 Specific heat capacity at constant pressure of saturated vapor R143a derived with the experimental values of the thermal diffusivity and with reference data for the thermal conductivity [3] and density [13].

Fig. 5 Sound velocity of saturated R143a.

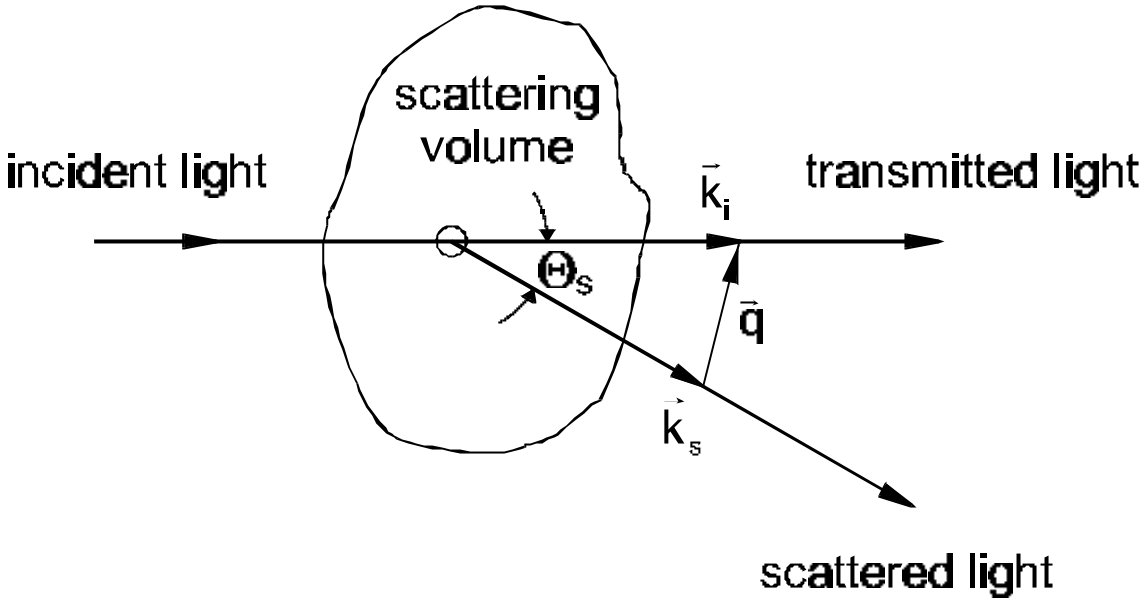

Fröba, Will, and Leipertz, Fig. 1

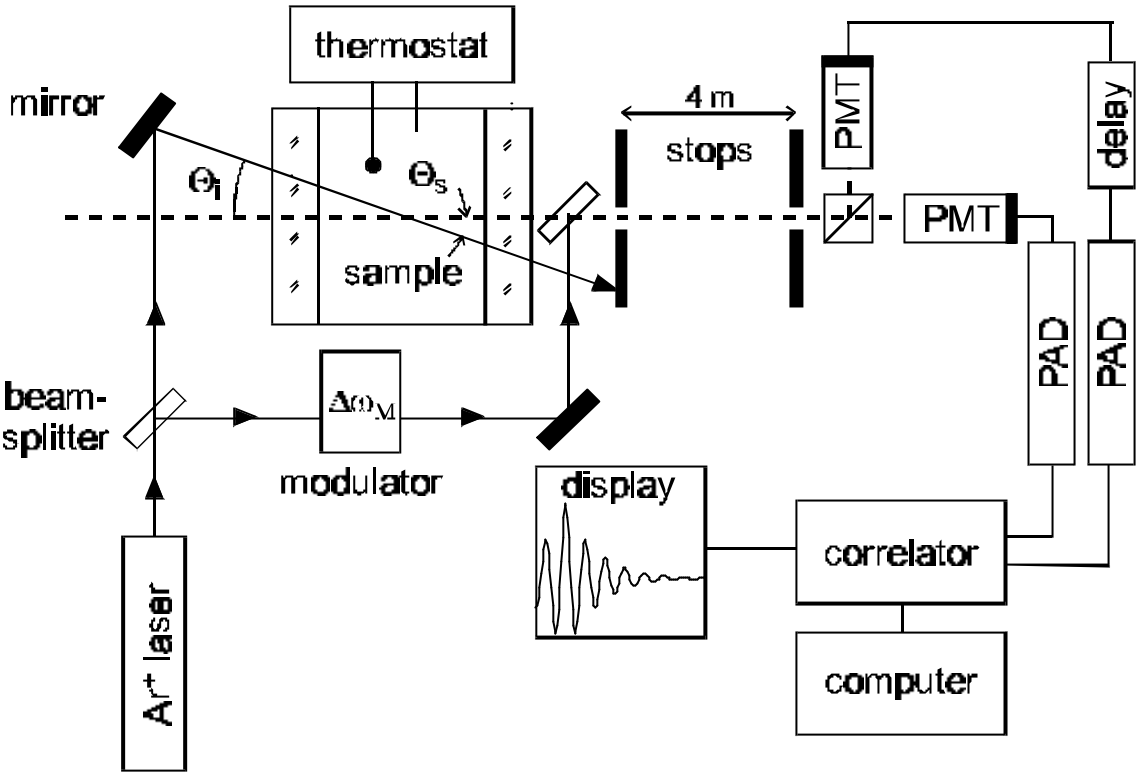

Fröba, Will, and Leipertz, Fig. 2

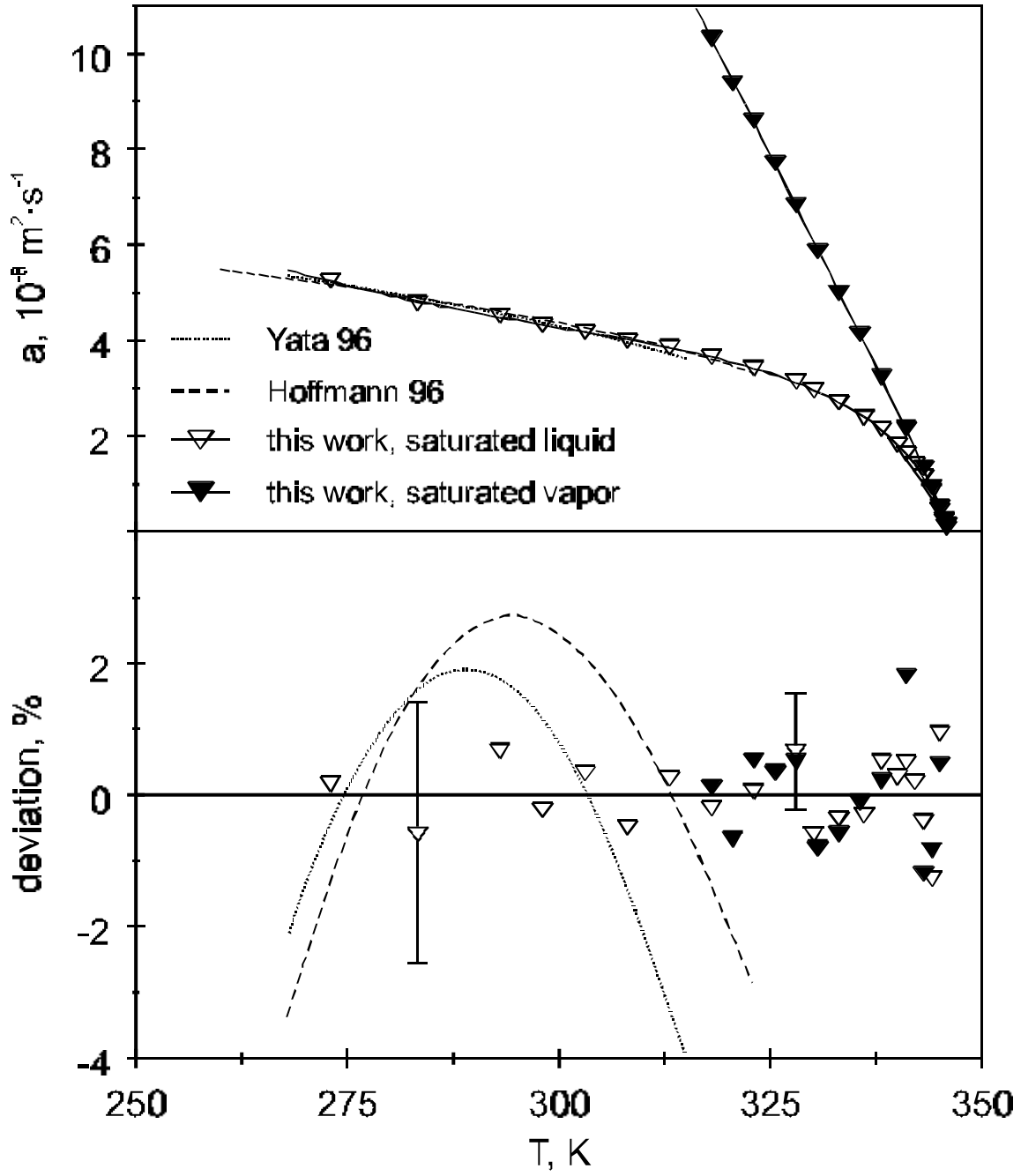

Fröba, Will, and Leipertz, Fig. 3

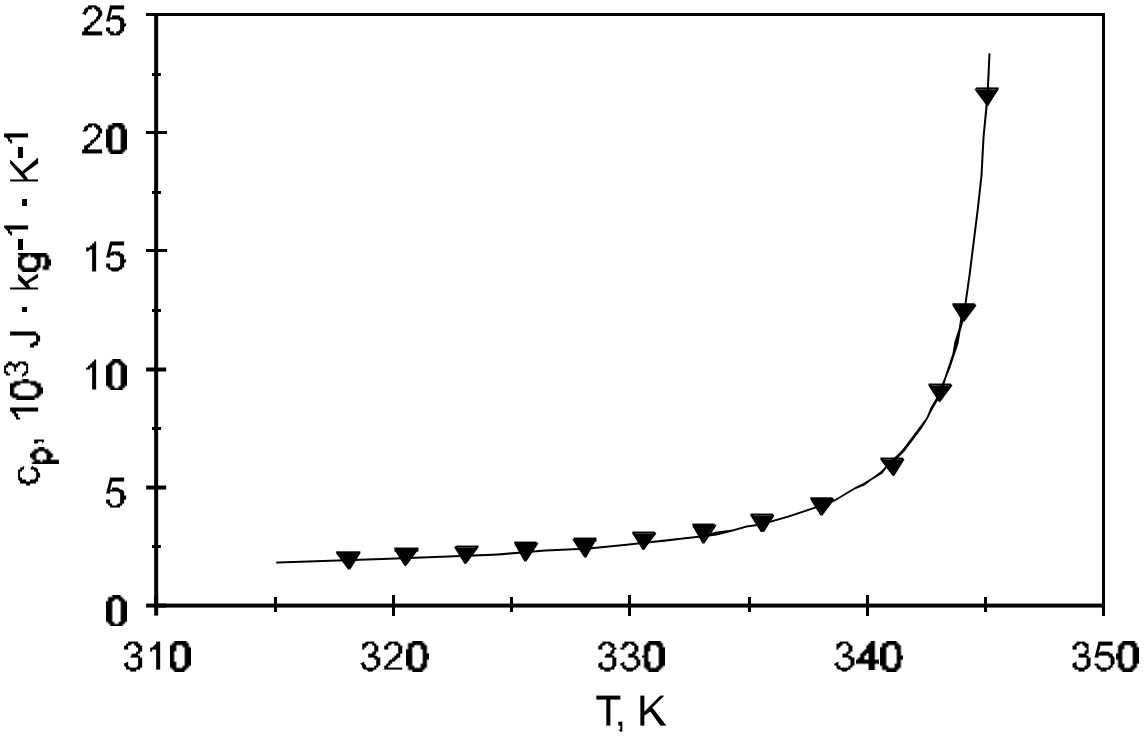

Fröba, Will, and Leipertz, Fig. 4

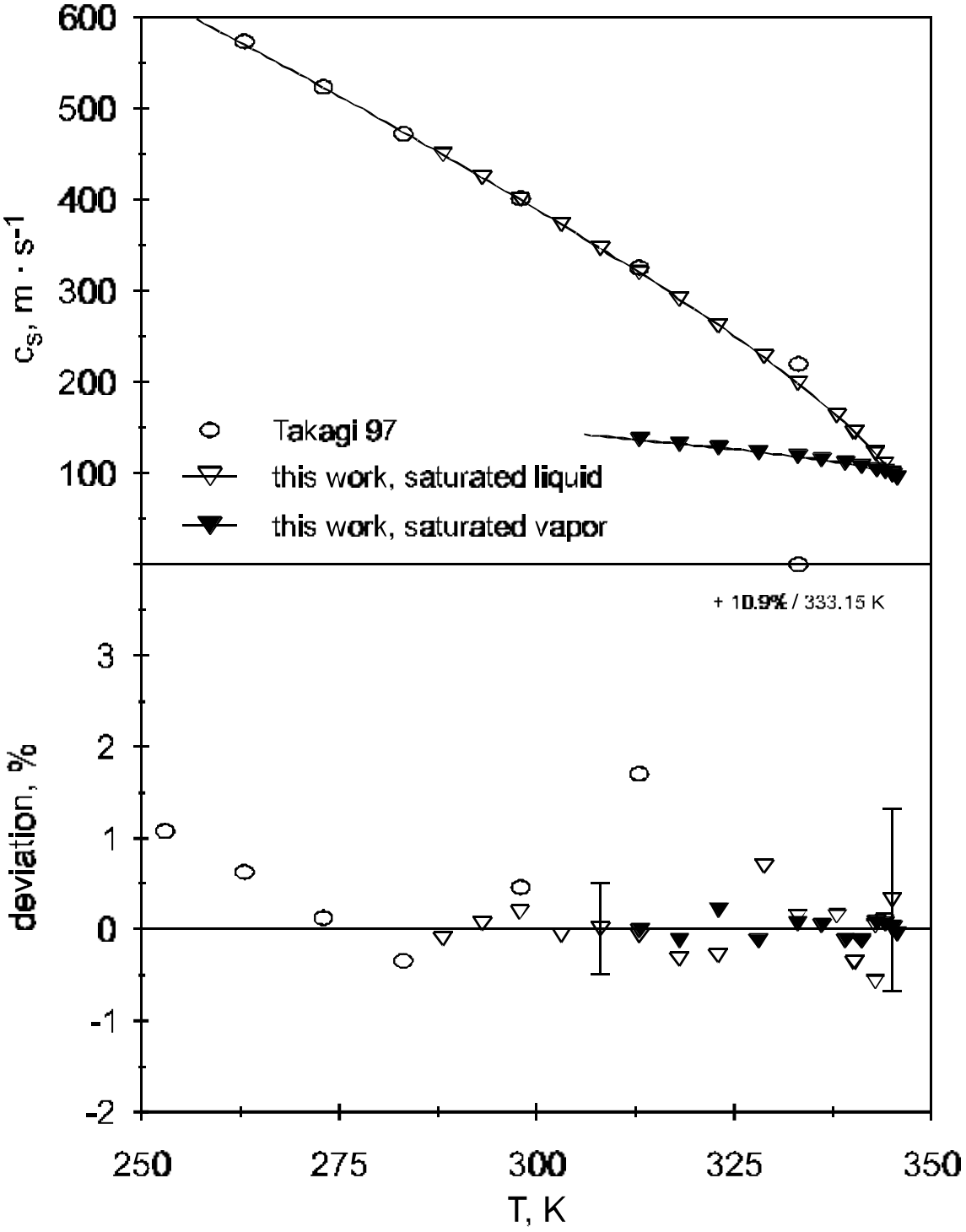

Fröba, Will, and Leipertz, Fig. 5